EMIC waves observed by the low-altitude satellite DEMETER during the November 2004 magnetic storm

D Píša, Michel Parrot, O Santolík, J. D. Menietti

AGU PUBLICATIONS

JGR

Journal of Geophysical Research: Space Physics

RESEARCH ARTICLE
10.1002/2014JA020233

EMIC waves observed by the low-altitude satellite DEMETER during the November 2004 magnetic storm

D. Píša[1,2,3], M. Parrot[2], O. Santolík[1,4], and J. D. Menietti[3]

[1]Institute of Atmospheric Physics, AS CR, Prague, Czech Republic, [2]LPC2E/CNRS, Orléans, France, [3]Department of Physics and Astronomy, University of Iowa, Iowa City, Iowa, USA, [4]Faculty of Mathematics and Physics, Charles University in Prague, Prague, Czech Republic

Abstract This paper presents an analysis of ULF (0–20 Hz) waves observed by the low-altitude satellite Detection of Electro-Magnetic Emissions Transmitted from Earthquake Regions (DEMETER) during the magnetic storm of November 2004. Since these ULF waves are measured by both electric and magnetic antennas, they may be identified as electromagnetic ion cyclotron (EMIC) waves. While EMIC waves have been previously observed in the low-altitude ionosphere, this is the first time that they are observed for such extensive time periods and at such high frequencies. A common feature of these emissions is that their observation region in the low-altitude ionosphere extends continuously from the high-latitude southern trough in one side up to the high-latitude northern trough. The analysis of wave propagation points to the possible source region placed in the inner magnetosphere ($L \sim 2-3$). Observed wave frequencies indicate that waves must be generated much farther from the Earth compared to the satellite orbit. Exceptionally high frequencies of about 10 Hz can be explained by the source region placed in the deep inner magnetosphere at $L \sim 2.5$. We hypothesize that these waves are generated below the local helium gyrofrequency and propagate over a large range of wave normal angles to reach low altitudes at $L \sim 1.11$. In order to investigate this scenario, a future study based on ray tracing simulations will be necessary.

Key Points:
- EMIC waves measured by DEMETER during the magnetic storm of November 2004
- EMIC waves observed over long period and on a large scale of latitudes
- Propagation of EMIC waves from the inner magnetosphere to low altitudes

Correspondence to:
D. Píša,
dp@ufa.cas.cz

Citation:
Píša, D., M. Parrot, O. Santolík, and J. D. Menietti (2015), EMIC waves observed by the low-altitude satellite DEMETER during the November 2004 magnetic storm, *J. Geophys. Res. Space Physics*, *120*, doi:10.1002/2014JA020233.

Received 29 MAY 2014
Accepted 10 JUN 2015
Accepted article online 12 JUN 2015

1. Introduction

The paper presents an analysis of electromagnetic waves observed by the satellite DEMETER (Detection of Electro-Magnetic Emissions Transmitted from Earthquake Regions). These waves were observed in the ULF range (0–20 Hz) in the upper ionosphere during a large magnetic storm. There is evidence that they might be related to electromagnetic ion cyclotron (EMIC) waves [e.g., *Cornwall*, 1965]. After initial satellite observation [*Russell et al.*, 1970; *Gurnett*, 1976; *Kintner and Gurnett*, 1977], EMIC waves have been extensively studied by both ground and satellite experiments. In auroral regions EMIC waves have been observed in connection with the intense electron fluxes by the S3-3 satellite [*Kintner et al.*, 1979; *Temerin and Lysak*, 1984], the Freja satellite [*Hamrin et al.*, 2002], the Fast satellite [*Chaston et al.*, 2002], and the Polar satellite [*Santolík et al.*, 2002b]. They have been also measured in the equatorial region at various altitudes by the GEOS satellites [*Young et al.*, 1981; *Rauch and Roux*, 1982], the DE 1 satellite [*Olsen et al.*, 1987], the Akebono satellite [*Sawada et al.*, 1991; *Kasahara et al.*, 1994; *Liu et al.*, 1994; *Sakaguchi et al.*, 2013], the Equator-S satellite [*Mouikis et al.*, 2002], the CRESS satellite [*Fraser and Nguyen*, 2001; *Meredith et al.*, 2003, 2014], the Cluster satellites [*Santolík et al.*, 2002a; *Pickett et al.*, 2010; *Grison et al.*, 2013; *Liu et al.*, 2013], and the Time History of Events and Macroscale Interactions during Substorms satellites [*Usanova et al.*, 2008, 2012]. During magnetic storms, an anisotropy in the pitch angle distribution of the ring current can occur in the equatorial region. The anisotropy drives the ion cyclotron instability from which the EMIC waves are generated [see, for example, *Bräysy et al.*, 1998; *Erlandson and Ukhorskiy*, 2001; *Mouikis et al.*, 2002; *Summers and Thorne*, 2003, and references therein]. They can be characterized by harmonic emission between the first multiples of the ion cyclotron frequency observed in both the electric and magnetic components. It is known that EMIC waves are responsible for electron precipitation in the inner magnetosphere [*Lorentzen et al.*, 2000; *Summers and Thorne*, 2003; *Meredith et al.*, 2003].

EMIC waves are also known to be propagated along steep density gradients of a plasmapause boundary to lower altitudes [e.g., *Thorne and Horne*, 1997]. Previous DEMETER observations in the vicinity of the plasmapause boundary show EMIC emissions detected during higher geomagnetic activity [*Parrot et al.*, 2006a, 2014]. EMIC waves can interact with the ring current ions which can be subsequently scattered into the ionosphere,

where they may modify the ionospheric conditions. These processes couple the magnetosphere with the ionosphere, and they can give rise to ULF waves propagating in the ionospheric waveguide [*Demekhov*, 2012]. Several active experiments showed that modulated heating of the ionosphere in the presence of natural currents (e.g., auroral electrojet) can initiate electromagnetic waves in the ELF band (3–3000 Hz) [*Ferraro et al.*, 1982; *McCarrick et al.*, 1990; *Moore et al.*, 2007; *Eliasson et al.*, 2012]. They have shown that these artificially triggered ELF emissions can propagate inside the Earth ionosphere waveguide to large distances with very little attenuation.

Our observations occur during the magnetic storm of November 2004. This particular storm was the strongest of the entire mission with minimum $Dst = -373$ nT and $Kp = 9$ occurring on 8 November 2004. This disturbed period also provided an opportunity to measure other new phenomena in the equatorial region [*Berthelier et al.*, 2008; *Malingre et al.*, 2008], in the trough [*Parrot et al.*, 2006a], or along the complete half orbits [*Pfaff et al.*, 2008; *Colpitts et al.*, 2012].

This paper reports observations attributed to EMIC waves recorded in the low-altitude ionosphere during this magnetic storm of 8–12 November 2004. Section 2 briefly describes the instrumentation, section 3 describes the observations, section 4 is devoted to discussion, and section 5 presents conclusions.

2. The Experiment

The French satellite DEMETER was launched on 29 June 2004, and the mission lasted to the end of December 2010. It was a three-axis stabilized spacecraft with a low-altitude (~710 km) polar and circular orbits. The orbit was subsequently lowered to 660 km in 2005. With nearly Sun-synchronous trajectory the satellite was covering regions in two local times. The ascending half orbits corresponded to nighttime (22:30 LT), and the descending half orbits corresponded to daytime (10:30 LT). Electromagnetic waves and plasma parameters were measured all around the Earth up to geomagnetic latitudes ±65°. The electric field experiment covered the frequency range from DC up to 3.5 MHz, whereas the magnetic field instrument measured from a few hertz up to 20 kHz. There were two different modes of operation of the satellite (survey and burst). During the survey mode, three-axis waveforms of the electric components up to 20 Hz were continuously recorded (the sampling frequency was ~39 Hz). When the instruments were operated in the burst mode, waveforms of all six components of the electromagnetic field were recorded in the ELF range up to 1.25 kHz with the sampling frequency 2.5 kHz. The burst mode allows spectral analysis with better time and frequency resolutions. It also enables the determination of the characteristics of wave propagation. Details of the wave experiment can be found in *Berthelier et al.* [2006] and *Parrot et al.* [2006b]. Throughout the paper a local geomagnetic coordinate system is used: the z axis is parallel with the ambient magnetic field line, the x axis lies in the orbital plane pointing outward away from the Earth, and the y axis completes the orthogonal system.

3. The Observations

All events studied here occurred within 09–12 November 2004 in the recovery phase of a large geomagnetic storm (with minimum $Dst = -373$ nT occurring on 8 November 2004). Figure 1 shows ULF data recorded on 10 November 2004 during a complete half orbit between 22:48:06 and 23:21:44 UT. The panels represent three components of the electric field. One can clearly see a broadband emission at a frequency of about 10 Hz in E_x and E_y components, while Figure 1 (bottom) for the E_z component, which is along the ambient magnetic field, does not show similar signature. This emission is observed practically all along the half orbit and is only limited at higher latitudes (in the north and in the south) by the ionospheric trough. The trough is identified by the rapid electron and ion density change (not shown) and the occurrence of the intense electrostatic turbulence (shown in Figure 1, time intervals 22:49–22:52 and 23:16–23:18). The solid, dashed, and dash-dotted white lines present the equatorial O^+, He^+, and H^+ cyclotron frequencies connected to the satellite position traced by using the International Geomagnetic Reference Field (IGRF) model [*Finlay et al.*, 2010]. There are no burst mode data available for this half orbit. During the analyzed time period 26 half orbits with similar emissions (as shown in Figure 1) were found. There are no such emissions observed during the onset of the geomagnetic storm on 8 November 2004.

Figure 2 represents ULF spectrograms observed on 11 November 2004. Spectrograms display several line bands which are approximately 2.5, 5, and 10 Hz. The frequency band near 5 Hz is observed along the major part of the orbit at low and middle latitudes, whereas the other frequency bands are observed over smaller

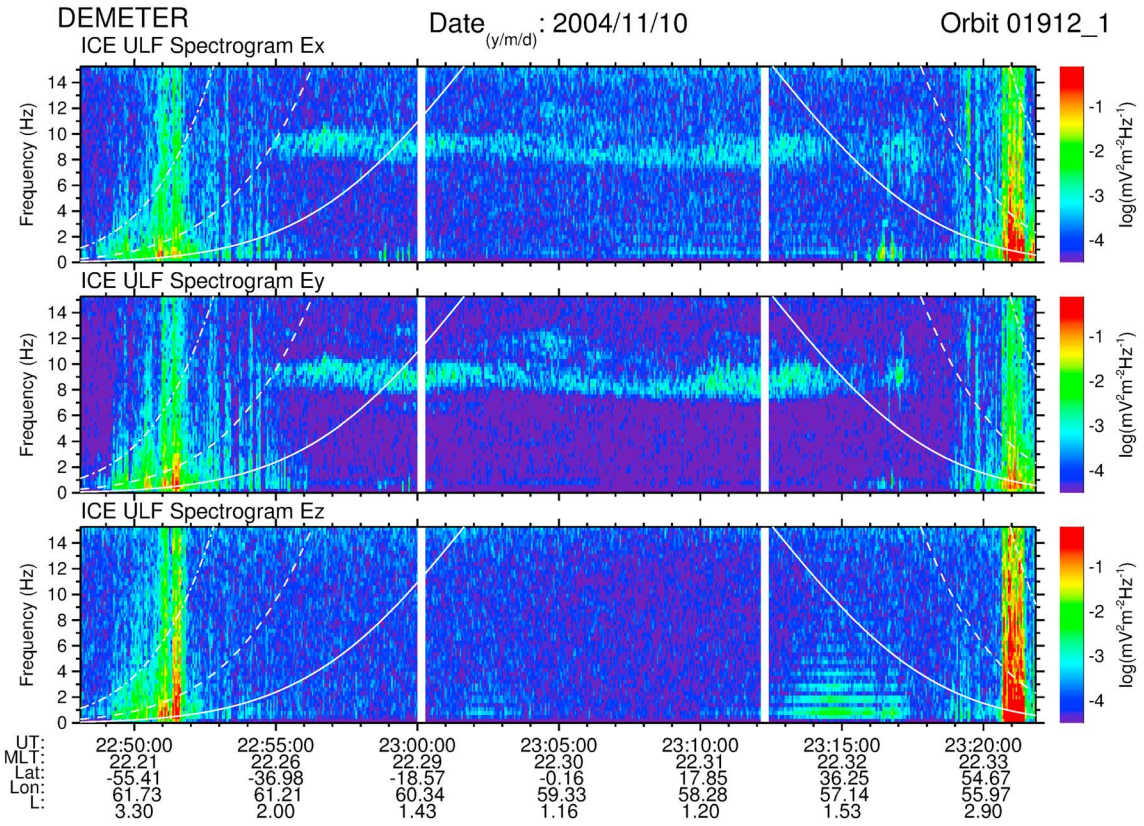

Figure 1. (from top to bottom) ULF spectrograms of the three electric components up to 15 Hz. The data are recorded on 10 November 2004 between 22:48:06 and 23:21:44 UT. The spectrogram intensity is color coded according to the scales on the right. The components are in a coordinate system linked to the Earth's magnetic field B_0 (E_z is along B_0). The parameters below are the universal time (UT), the magnetic local time (MLT), the geomagnetic latitude and longitude, and McIlwain parameter (L). The vertical white lines indicate data gaps due to calibration. The set of lines observed in Figure 1 (bottom) around 23:15:00 UT at frequencies less than 5 Hz is due to interferences. The solid, dashed, and dash-dotted white lines indicate equatorial O^+, He^+, and H^+ cyclotron frequencies traced from the satellite position.

parts of the orbit in the north (10 Hz) and in the south (2.5 Hz). For this half orbit, the burst mode is available between 06:23:33 and 06:28:58 UT. Detailed wave propagation analysis of ELF waveforms for three magnetic field components and three electric field components up to 20 Hz is shown in Figure 3. Figures 3a and 3b, respectively, represent high-resolution power spectrograms of magnetic and electric field fluctuations. The polar angle of the wave vector presented in Figure 3c has been obtained by the singular value decomposition (SVD) method [*Santolík et al.*, 2003] in the coordinate system linked to the ambient terrestrial magnetic field B_0. Figures 3d and 3e show the sense of polarization of the magnetic and electric components, respectively, with a level of confidence, i.e., normalized by its standard deviation, also using the SVD method. Negative values mean left-hand polarized field, positive values correspond to the right-handed polarization, and values between −1 and +1 indicate a low confidence level. Figure 3f presents the polar angle of the Poynting flux with respect to the ambient magnetic field. It can be seen that the same broadband emissions appear both on the electric and on the magnetic spectrograms centered at frequencies of about 6 Hz and 12 Hz. The satellite was on the dayside (∼11:00 LT) moving from the north to the south. The polar angle of the wave vector at both frequencies is rising with descending geomagnetic latitude and reaching angle ∼90° below a latitude of ∼15°. The polarization of the magnetic field is significantly right handed for higher latitudes, and it is more mixed when reaching lower latitudes. The polarization of the electric field is dominantly right handed throughout the whole interval for both frequencies. The polar angle of the Poynting vector is rising with descending latitude and reaches a value of ∼90° below a latitude of ∼15°, i.e., energy propagates perpendicular with respect to the ambient magnetic field.

The wave propagation analysis for all available data with the ULF wave signature observed in the burst mode between 9 and 12 November 2004 is shown in Figure 4. For this purpose, spectral matrices of all six components of electromagnetic field fluctuations [*Santolík et al.*, 2003] with time resolution of 4 s and frequency

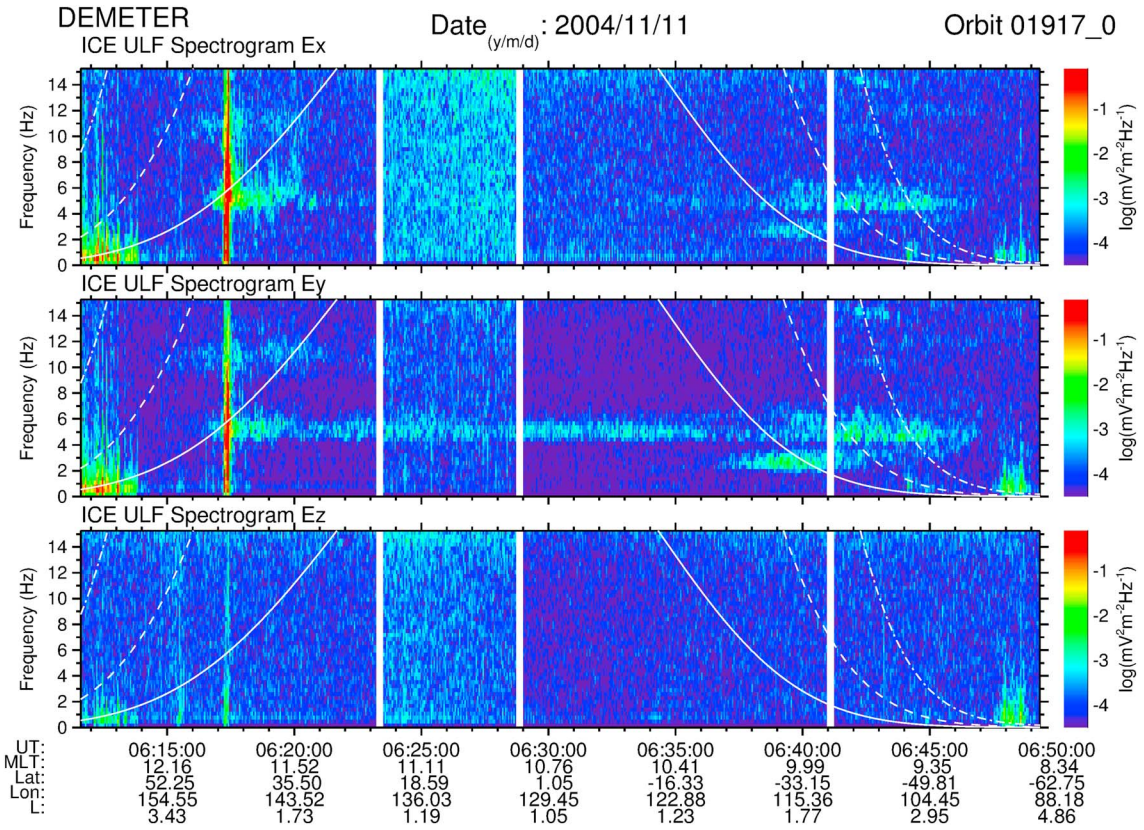

Figure 2. Same representation as Figure 1 but observed on 11 November 2004 between 06:11:36 UT and 06:49:14 UT. The vertical white lines at ~06:23 and 06:29 indicate the time intervals where instruments were operated in the burst mode. The white line at ~06:42 shows a data gap.

resolution of 3.7 Hz have been calculated. For each time interval, the frequency with a maximum power in the magnetic field component was selected. The dynamics of the wave amplitudes for the observed events is typically in a range of 10–100 μV m^{-1} for the electric field and 1–10 pT for the magnetic field, respectively. All dependencies are plotted as a function of geomagnetic latitude. The dayside and the nightside half orbits are shown by red and black crosses, respectively. The wave normal directions (Figures 4a and 4b) were computed through the SVD method. $Theta_k$ is defined as the polar angle between the wave vector and the magnetic field, 0° for parallel and 180° for antiparallel propagation with respect to the magnetic field. Phi_k defines an azimuthal angle between the wave vector and magnetic field, 0° (180°) for a direction outward (toward) the Earth. The wave normal angle for dayside half orbits and positive latitudes decreases with increasing latitude. For negative latitudes we have a few observations showing wave normal angles almost antiparallel to the magnetic field. Nightside observations are only obtained for higher latitudes and show more scattered wave normal angles. Both data sets show azimuthal angles which correspond to propagation from the magnetosphere toward the Earth. The ellipticity can be defined as the ratio of the two axes of the polarization ellipse and gives values from −1 to 1. The polarization can be estimated from the sign for the ellipticity plotted in Figure 4c. The polarization is mostly right handed for the dayside observations and mixed for the nightside data. Figure 4d presents a variation of the polar angle for the Poynting vector with respect to the ambient magnetic field. Polar angle for both data sets and positive latitudes decreases with increasing latitude. For lower positive latitudes, waves propagate almost perpendicular to the magnetic field, whereas for higher latitudes waves are more field aligned. For negative latitudes on the dayside, the polar angle is almost antiparallel to the magnetic field.

For a better visualization, wave normal and Poynting vector directions for the daytime observations from Figures 4a and 4d (red crosses) are plotted as a function of the geomagnetic latitude in Figure 5. Both wave normal vector (black arrow) and the Poynting vector (red arrow) are projected to the meridional plane at MLT=11 h with a step of 5°in the geomagnetic latitude. The projection of the IGRF model is shown by light

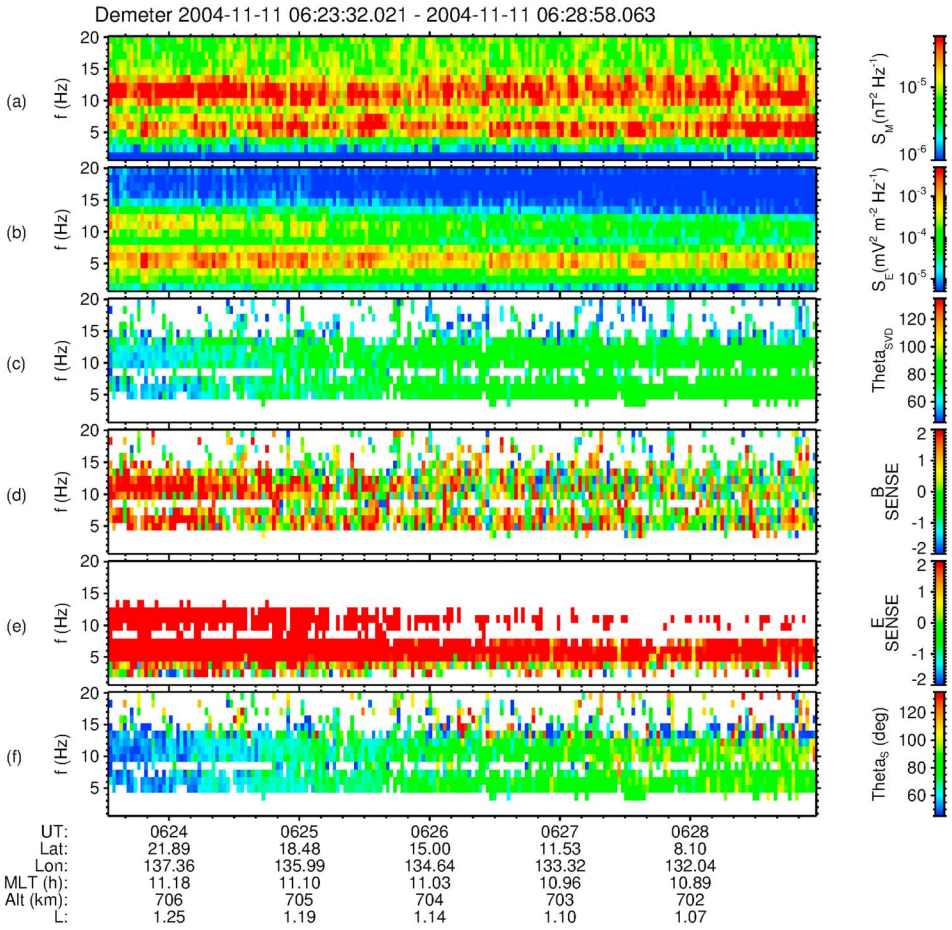

Figure 3. (a and b) Sum of the power spectral densities of the three measured magnetic field components and three measured electric field components, respectively, according to the color bars at the right-hand side, in the frequency range up to 40 Hz. (c) Polar angle Theta$_k$, 0° for waves propagating parallel to magnetic field and 180° for waves propagating antiparallel to magnetic field. (d) Sense of polarization of the wave magnetic field with a level of confidence using the method of singular value decomposition (SVD) of the magnetic spectral matrix [*Santolík et al.*, 2003]. (e) Sense of polarization of the wave electric field with a level of confidence. (f) Polar angle of the Poynting flux with respect to the local field line of the ambient magnetic field, 0° indicating the same direction and 180° the opposite direction.

gray lines. The dashed black line represents the projection of the satellite's orbit. This analysis points to a possible source region in the magnetosphere instead of the top of the ionosphere.

4. Discussions

In this study we examine ULF data from the DEMETER satellite during the November 2004 magnetic storm. This was the strongest geomagnetic storm during the entire mission. The analyzed observations are therefore unique for the DEMETER mission. During the rest of the mission the geomagnetic activity was very quiet, with only a few exceptions. For this reason there was no similar opportunity to observe EMIC-like fluctuations at such high frequencies and in a large range of geomagnetic latitudes.

Past observations in the same region have shown that similar harmonic structures might be related to EMIC waves. Using Magsat data, *Iyemori and Hayashi* [1989] have observed PC1 waves at ionospheric altitudes (350–550 km) at 58°–60° invariant latitude which is close to the plasmapause position. *Erlandson et al.* [1993] have reported low-frequency (0.5–4.0 Hz) electromagnetic ion cyclotron waves observations by the DE 2 satellite at magnetic latitudes from 57 to 60° and altitudes from 600 to 900 km. With the same data, *Erlandson and Anderson* [1996] have performed a statistical analysis which indicates that most events were observed at frequencies between 0.4 and 2.0 Hz, in the dawn (0400–0600 MLT) and noon (1000–1500 MLT) sectors, and

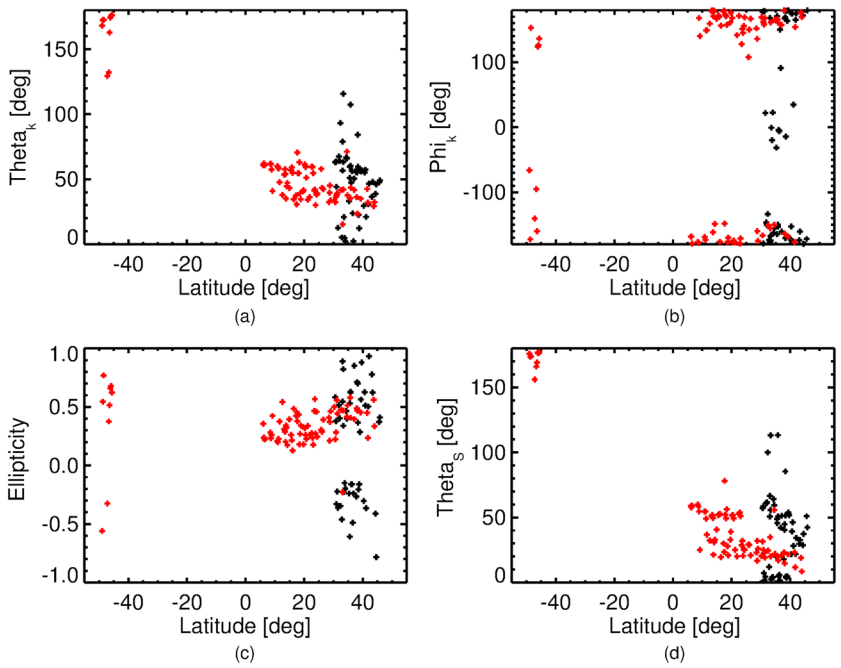

Figure 4. Wave propagation properties derived from all burst mode observations between 9 and 12 November 2004. Data are divided into two groups for the dayside (red points) and nightside (black points) half orbits. (a) Polar angle Theta$_k$ and (b) azimuthal angle Phi$_k$ of the wave vector; (c) ellipticity and (d) polar angle of the Poynting flux as a function of geomagnetic latitude.

from 50° to 62° invariant latitude [see also *Iyemori et al.*, 1994]. These previous low-altitude missions reported EMIC waves observed only during time periods up to a maximum of 1 min at high invariant latitudes (50–60°).

The ion cyclotron frequencies calculated along the satellite's orbit from the fluxgate magnetometer data for a hydrogen, helium, and oxygen are in the range of 300–600 Hz, 75–163 Hz, and 19–35 Hz, respectively. Therefore, ULF emissions observed by the DEMETER satellite were not detected at ion cyclotron frequencies related to the local magnetic field. The wave normal and Poynting flux angles plotted in Figures 4a and 4d show that with increasing latitude these angles are decreasing. The azimuthal angles of the wave normal for most of the events, especially at the dayside, show propagation from the magnetosphere to the Earth (±180°). Although it was shown in the past [e.g., *Demekhov*, 2012] that ULF/ELF wave sources can exist in the ionosphere, our analysis of wave normal and Poynting vector directions point to a source region which would be more likely located in the inner magnetosphere. The source position is consistent with the generally accepted model for EMIC waves, which are generated in the inner magnetosphere close to the plasmapause boundary [e.g., *Cornwall*, 1965].

The similar magnetospheric conditions as those for the DEMETER observations were met during the Akebono mission. *Sakaguchi et al.* [2013] show EMIC waves at the frequency of about 8 Hz related to a severe geomagnetic storm (with *Dst* minimum −255 nT occurring on 19 September 1989) observed by the Akebono satellite ($L \sim 2.5–5$) in September 1989. After the onset and at the beginning of recovery phase, the plasmapause was pushed toward the Earth reaching field lines ($L \sim 2.5–3\ R_E$) where the He^+ cyclotron frequency is about 10 Hz. A magnetic activity-dependent model of the plasmapause position [*O'Brien and Moldwin*, 2003] consistent with conditions for 10 November 2004 is presented in Figure 5 and shows a compression reaching radial distances about of 2 R_E for the local time around 10:30. The plasmapause was probably located closer to the Earth, and therefore waves from the source region generated close to the He^+ cyclotron frequency can be observed by DEMETER.

In a single-ion cold plasma approximation, EMIC waves can propagate at frequencies below the H^+ cyclotron frequency as the guided (field-aligned) left-hand polarized and unguided right-hand polarized waves [*Young et al.*, 1981; *Rauch and Roux*, 1982; *Fraser*, 1985]. An occurrence of heavy ions such as He^+ and O^+ causes the wave modes to be more complicated, with two additional resonances, two cutoffs, and two crossover frequencies [*Gurnett et al.*, 1965]. This is visualized in Figure 6. For the wave vector parallel with the ambient

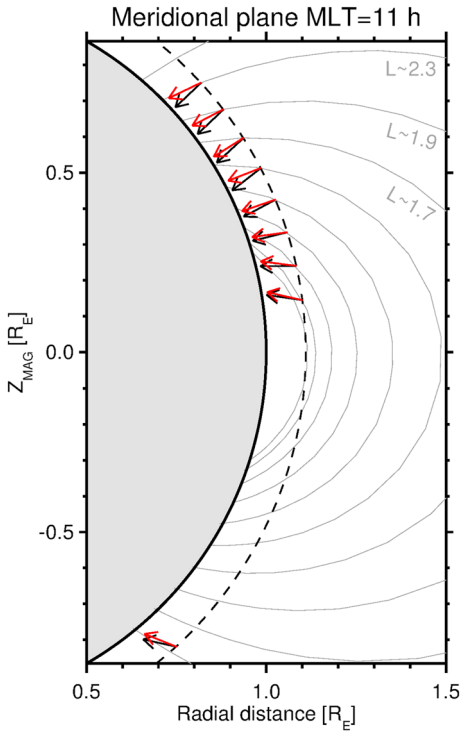

Figure 5. Directions of the wave normal (black arrow) and the Poynting vector (red arrow) projected to the plane of the magnetic meridian at MLT = 11 h. Dayside burst mode observations between 9 and 12 November 2004 (red points from Figure 4) with the 5° step in the geomagnetic latitude are plotted. The black dashed line shows the projected altitude of DEMETER. Light gray lines represent a projection of the IGRF geomagnetic field.

magnetic field, Theta$_k$ = 0°, the left-hand mode has three resonances at each ion cyclotron frequency. There are three stop bands between cyclotron frequency and *L*-mode cutoff. The right-hand mode is unaffected. At the crossover frequency the left-hand and right-hand branches cross each other. For oblique angles of the wave vector, 0° < Theta$_k$ < 90°, the sense of polarization changes between right- and left-handed modes at the crossover frequency. At this frequency a polarization reversal occurs. For the wave vector perpendicular to the ambient magnetic field, Theta$_k$ = 90°, waves in the left-hand mode can only propagate between crossover and *L*-mode cutoff. The right-hand mode has stop band between bi-ion hybrid resonance and crossover frequency. For more detailed description see, for example, *Rauch and Roux* [1982].

We suggest that for our case, left-hand polarized wave could be generated below the He^+ cyclotron resonance. The presence of O^+ ions leads to a change of polarization, at the crossover frequency (f_{cr}), where the waves become right-hand polarized. The right-hand polarization allows waves with $f < f_{cr}$ to propagate across the left-hand mode cutoff above the O^+ cyclotron frequency. This is supported by the theoretical model of polarization change in a multicomponent plasma [*Rauch and Roux*, 1982; *Perraut et al.*, 1984] and is in agreement with previous observations [e.g., *Young et al.*, 1981; *Rauch and Roux*, 1982] and more recently from the Cluster observations [*Liu et al.*, 2013].

DEMETER observations also show similar emissions detected in high-latitude regions (50–60°) of the ionospheric trough (as presented in Figure 1). Sources for these waves are known to be close to the equatorial region at the plasmapause boundary ($L \sim 2.5$–$5\ R_E$) [*Yizengaw et al.*, 2005]. Waves then propagate to higher latitudes along the density gradient near the plasmasphere boundary [*Kasahara et al.*, 1992, 1994; *Thorne and Horne*, 1997; *Fraser and Nguyen*, 2001]. For these

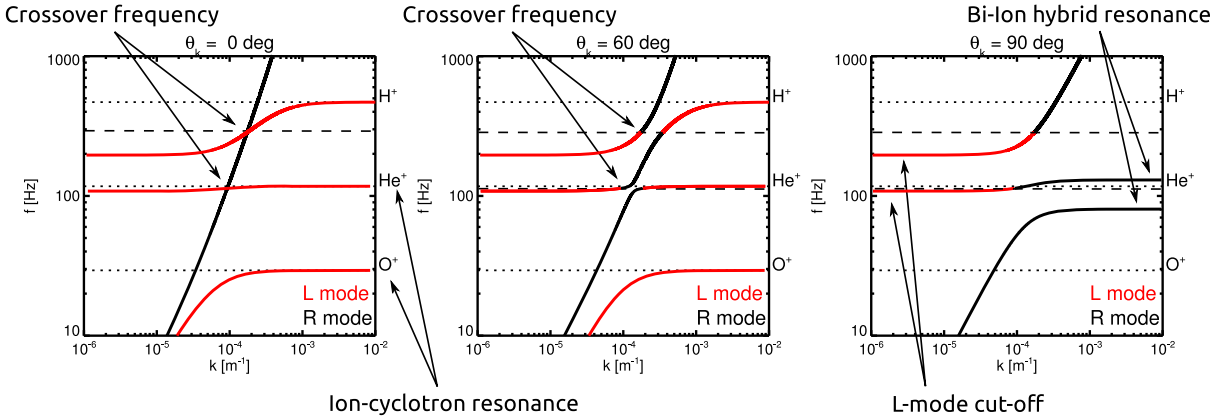

Figure 6. Dispersion relation of ULF waves in the presence of three ion species (H^+ 64%, He^+ 2%, and O^+ 34%) in the cold plasma approximation. Propagation with an angle of a wave vector with respect to the ambient magnetic field equal to (left) 0, (middle) 60, and (right) 90°are shown. Left-hand and right-hand modes are plotted by the red and black lines, respectively. Ion cyclotron frequencies are represented by black dotted lines. The crossover frequency is shown by the black dashed line. The overall plasma density at MLT = 12 h, geomagnetic latitude = 0°, and radial distance = 1.11 R_E (satellite's altitude at geomagnetic equator) is obtained from the global plasma core model [*Gallagher et al.*, 2000].

reasons we propose that the waves measured by DEMETER at higher latitudes might also be identified as EMIC waves. Similar waves at ion cyclotron harmonics were observed in the auroral zone, for example, by *Chaston et al.* [2002] and *Santolík et al.* [2002a].

Our analysis suggests that the observed waves could be generated below the He^+ cyclotron resonance. These emissions are typically observed at frequencies around 2.5, 5, and 10 Hz, which can be due to the helium harmonics. *Kokubun et al.* [1991] have observed harmonics of the helium gyrofrequency with EXOS-D data, and during a magnetic storm *Liu et al.* [1994] have observed bands at the harmonics of the oxygen gyrofrequency.

A backward ray tracing simulation is needed to thoroughly analyze the wave propagation and possible locations of the source region. This analysis can be based on the above presented in situ measurements of EMIC waves. The simulation procedure can be initialized by the measured wave vector directions at the DEMETER altitude. We have tried to perform initial steps in this analysis, but it became clear that wavelengths at these frequencies can be sometimes larger than spatial scales for changes of the refractive index. Particularly, this problem as been encountered for oblique propagation through a region where the wave frequency is close to the ion cyclotron frequency. This fact introduces additional difficulties to any raypath simulation, and a proper analysis goes far beyond the scope of this paper.

5. Conclusions

We present observations of ULF waves from the DEMETER satellite during the magnetic storm. The November 2004 magnetic storm was the strongest during the entire DEMETER mission. Our results propose that waves may be identified as EMIC waves. Although these emissions have been already reported by previous low-altitude missions at higher latitudes, the new finding with DEMETER data is that these EMIC waves are observed over a long period and on a large scale of latitudes in the low-altitude ionosphere. The previous low-altitude missions present EMIC wave observations only during time periods up to a maximum of 1 min. It was shown in the past that ULF/ELF wave sources can exist in the ionosphere as well, but our measurements of wave normal and Poynting vector directions point to a source region which would be more likely located in the magnetosphere. A speculative scenario could be based on a possible origin at the plasmapause equatorial boundary. In our case, this boundary would be pushed closer toward the Earth due to a large geomagnetic storm. The waves might then penetrate down to the low-altitude ionosphere by crossing the polarization reversal region. Consequently, EMIC waves are observed as right-handed polarized waves onboard the DEMETER satellite. Future study based on ray tracing simulations is needed in order to investigate this suggested scenario.

Acknowledgments

The work of D.P. and M.P. in LPC2E Orléans was supported by the Centre National d'Etudes Spatiales (CNES). Observations of the electric field experiment ICE and with the magnetic field experiment IMSC embarked on DEMETER are available on http://cdpp.eu/. The authors thank J.J. Berthelier, the PI of the electric field and plasma experiment, for the use of the data. This work was also supported by MSMT grants LH14010 and LH12231 and by AVCR international project M100421206 and Premium Academiae award.

M. Balikhin thanks two anonymous reviewers for their assistance in evaluating this paper.

References

Berthelier, J., et al. (2006), ICE, the electric field experiment on DEMETER, *Planet. Space Sci.*, *54*, 456–471, Elsevier.

Berthelier, J. J., M. Malingre, R. Pfaff, E. Seran, R. Pottelette, J. Jasperse, J. P. Lebreton, and M. Parrot (2008), Lightning-induced plasma turbulence and ion heating in equatorial ionospheric depletions, *Nat. Geosci.*, 101–105, doi:10.1038/ngeo109.

Bräysy, T., K. Mursula, and G. Marklund (1998), Ion cyclotron waves during a great magnetic storm observed by Freja double-probe electric field instrument, *J. Geophys. Res.*, *103*(A3), 4145–4155, doi:10.1029/97JA02820.

Chaston, C., J. W. Bonnell, J. P. McFadden, R. E. Ergun, and C. W. Carlson (2002), Electromagnetic ion cyclotron waves at proton cyclotron harmonics, *J. Geophys. Res.*, *107*(A11), 1351, doi:10.1029/2001JA900141.

Colpitts, C. A., C. A. Cattell, J. U. Kozyra, and M. Parrot (2012), Satellite observations of banded VLF emissions in conjunction with energy-banded ions during very large geomagnetic storms, *J. Geophys. Res.*, *117*, A10211, doi:10.1029/2011JA017329.

Cornwall, J. M. (1965), Cyclotron instabilities and electromagnetic emission in the ultra low frequency and very low frequency ranges, *J. Geophys. Res.*, *70*, 61–69, doi:10.1029/JZ070i001p00061.

Demekhov, A. G. (2012), Coupling at the atmosphere-ionosphere-magnetosphere interface and resonant phenomena in the ULF range, *Space Sci. Rev.*, *168*, 595–609, doi:10.1007/s11214-011-9832-6.

Eliasson, B., C.-L. Chang, and K. Papadopoulos (2012), Generation of ELF and ULF electromagnetic waves by modulated heating of the ionospheric *F*2 region, *J. Geophys. Res.*, *117*, A10320, doi:10.1029/2012JA017935.

Erlandson, R. E., and B. J. Anderson (1996), Pc 1 waves in the ionosphere: A statistical study, *J. Geophys. Res.*, *101*(A4), 7843–7857, doi:10.1029/96JA00082.

Erlandson, R. E., and A. J. Ukhorskiy (2001), Observations of electromagnetic ion cyclotron waves during geomagnetic storms: Wave occurrence and pitch angle scattering, *J. Geophys. Res.*, *106*(A3), 3883–3895, doi:10.1029/2000JA000083.

Erlandson, R. E., T. L. Aggson, W. R. Hogey, and J. A. Slavin (1993), Simultaneous observations of subauroral electron temperature enhancements and electromagnetic ion cyclotron waves, *Geophys. Res. Lett.*, *20*(16), 1723–1726, doi:10.1029/93GL01975.

Ferraro, A. J., H. S. Lee, R. A. Allshouse, K. Carroll, A. A. Tomko, F. J. Kelly, and R. G. Joiner (1982), VLF/ELF radiation from the ionospheric dynamo current system modulated by powerful HF signals, *J. Atmos. Terr. Phys.*, *44*, 1113–1122.

Finlay, C. C., et al. (2010), International geomagnetic reference field: The eleventh generation, *Geophys. J. Int.*, *183*, 1216–1230, doi:10.1111/j.1365-246X.2010.04804.x.

Fraser, B., and T. Nguyen (2001), Is the plasmapause a preferred source region of electromagnetic ion cyclotron waves in the magnetosphere?, *J. Atmos. Sol. Terr. Phys.*, *63*, 1225–1247.

Fraser, B. J. (1985), Observations of ion cyclotron waves near synchronous orbit and on the ground, *Space Sci. Rev.*, *42*, 357–374, doi:10.1007/BF00214993.
Gallagher, D. L., P. D. Craven, and R. H. Comfort (2000), Global core plasma model, *J. Geophys. Res.*, *105*, 18,819–18,833, doi:10.1029/1999JA000241.
Grison, B., O. SantolíK, N. Cornilleau-Wehrlin, A. Masson, M. J. Engebretson, J. S. Pickett, Y. Omura, P. Robert, and R. Nomura (2013), EMIC triggered chorus emissions in Cluster data, *J. Geophys. Res. Space Physics*, *118*, 1159–1169, doi:10.1002/jgra.50178.
Gurnett, D. (1976), Plasma wave interaction with energetic ions near the magnetic equator, *J. Geophys. Res.*, *81*(16), 2765–2770.
Gurnett, D. A., S. D. Shawhan, N. M. Brice, and R. L. Smith (1965), Ion cyclotron whistlers, *J. Geophys. Res.*, *70*, 1665–1688, doi:10.1029/JZ070i007p01665.
Hamrin, M., P. Norqvist, M. André, and A. Eriksson (2002), A statistical study of wave properties and electron density at 1700 km in the auroral region, *J. Geophys. Res.*, *107*(A8), SIA 21–1–SIA 21–13, doi:10.1029/2001JA900144.
Iyemori, T., and K. Hayashi (1989), PC 1 micropulsations observed by Magsat in the ionospheric *F* region, *J. Geophys. Res.*, *94*(A1), 93–100, doi:10.1029/JA094iA01p00093.
Iyemori, T., M. Sugiura, A. Oka, Y. Morita, M. Ishii, J. A. Slavin, L. H. Brace, R. A. Hoffman, and J. D. Winningham (1994), Localized injection of large-amplitude Pc 1 waves and electron temperature enhancement near the plasmapause observed by DE 2 in the upper ionosphere, *J. Geophys. Res.*, *99*(A4), 6187–6199, doi:10.1029/93JA02750.
Kasahara, Y., A. Sawada, M. Yamamoto, I. Kimura, S. Kokubun, and K. Hayashi (1992), Ion cyclotron emissions observed by the satellite Akebono in the vicinity of the magnetic equator, *Radio Sci.*, *27*, 347–362.
Kasahara, Y., H. Kenmochi, and I. Kimura (1994), Propagation characteristics of the ELF emissions observed by the satellite Akebono in the magnetic equatorial region, *Radio Sci.*, *29*(4), 751–767.
Kintner, P., and D. Gurnett (1977), Observations of ion cyclotron waves within the plasmasphere by Hawkeye 1, *J. Geophys. Res.*, *82*(16), 2314–2318.
Kintner, P. M., M. C. Kelley, R. D. Sharp, A. G. Ghielmetti, M. Temerin, C. Cattell, P. F. Mizera, and J. F. Fennell (1979), Simultaneous observations of energetic (keV) upstreaming and electrostatic hydrogen cyclotron waves, *J. Geophys. Res.*, *84*, 7201–7212, doi:10.1029/JA084iA12p07201.
Kokubun, S., M. Takami, K. Hayashi, H. Fukunishi, I. Kimura, A. Sawada, and Y. Kasahara (1991), Triaxial search coil measurements of ELF waves in the plasmasphere: Initial results from EXOS-D, *Geophys Res. Lett.*, *18*(2), 301–304, doi:10.1029/90GL02599.
Liu, H., S. Kokubun, and K. Hayashi (1994), Equatorial electromagnetic emission with discrete spectra near harmonics of oxygen gyrofrequency during magnetic storm, *Geophys. Res. Lett.*, *21*(3), 225–228, doi:10.1029/93GL02836.
Liu, Y. H., B. J. Fraser, and F. W. Menk (2013), EMIC waves observed by Cluster near the plasmapause, *J. Geophys. Res. Space Physics*, *118*, 5603–5615, doi:10.1002/jgra.50486.
Lorentzen, K. R., M. McCarthy, G. Parks, J. Foat, R. Millan, D. Smith, R. Lin, and J. Treilhou (2000), Precipitation of relativistic electrons by interaction with electromagnetic ion cyclotron waves, *J. Geophys. Res.*, *105*(A3), 5381–5390, doi:10.1029/1999JA000283.
Malingre, M., J.-J. Berthelier, R. Pfaff, J. Jasperse, and M. Parrot (2008), Lightning-induced lower-hybrid turbulence and trapped Extremely Low Frequency (ELF) electromagnetic waves observed in deep equatorial plasma density depletions during intense magnetic storms, *J. Geophys. Res.*, *113*, A11320, doi:10.1029/2008JA013463.
McCarrick, M. J., A. Y. Wong, R. F. Wuerker, B. Chouinard, and D. D. Sentman (1990), Excitation of ELF waves in the Schumann resonance range by modulated HF heating of the polar electrojet, *Radio Sci.*, *25*, 1291–1298, doi:10.1029/RS025i006p01291.
Meredith, N., R. Thorne, R. Horne, D. Summers, B. Fraser, and R. Anderson (2003), Statistical analysis of relativistic electron energies for cyclotron resonance with EMIC waves observed on CRRES, *J. Geophys. Res.*, *108*(A6), 1250, doi:10.1029/2002JA009700.
Meredith, N. P., R. B. Horne, T. Kersten, B. J. Fraser, and R. S. Grew (2014), Global morphology and spectral properties of EMIC waves derived from CRRES observations, *J. Geophys. Res. Space Physics*, *119*, 5328–5342, doi:10.1002/2014JA020064.
Moore, R. C., U. S. Inan, T. F. Bell, and E. J. Kennedy (2007), ELF waves generated by modulated HF heating of the auroral electrojet and observed at a ground distance of 4400 km, *J. Geophys. Res.*, *112*, A05309, doi:10.1029/2006JA012063.
Mouikis, C., et al. (2002), Equator-S observations of He^+ energization by EMIC waves in the dawnside equatorial magnetosphere, *Geophys. Res. Lett.*, *29*(10), 74–1–74–4, doi:10.1029/2001GL013899.
O'Brien, T. P., and M. B. Moldwin (2003), Empirical plasmapause models from magnetic indices, *Geophys. Res. Lett.*, *30*(4), 1152, doi:10.1029/2002GL016007.
Olsen, R. C., S. D. Shawhan, D. L. Gallagher, J. L. Green, C. R. Chappell, and R. R. Anderson (1987), Plasma observations at the Earth's magnetic equator, *J. Geophys. Res.*, *92*(A3), 2385–2407, doi:10.1029/JA092iA03p02385.
Parrot, M., A. Buzzi, O. Santolík, J. J. Berthelier, J. A. Sauvaud, and J. P. Lebreton (2006a), New observations of electromagnetic harmonic ELF emissions in the ionosphere by the DEMETER satellite during large magnetic storms, *J. Geophys. Res.*, *111*, A08301, doi:10.1029/2005JA011583.
Parrot, M., et al. (2006b), The magnetic field experiment IMSC and its data processing onboard DEMETER: Scientific objectives, description and first results, *Planet. Space Sci.*, *54*(5), 441–455.
Parrot, M., F. Němec, and O. Santolík (2014), Analysis of fine ELF wave structures observed poleward from the ionospheric trough by the low-altitude satellite DEMETER, *J. Geophys. Res. Space Physics*, *119*, 2052–2060, doi:10.1002/2013JA019557.
Perraut, S., R. Gendrin, A. Roux, and C. de Villedary (1984), Ion cyclotron waves—Direct comparison between ground-based measurements and observations in the source region, *J. Geophys. Res.*, *89*, 195–202, doi:10.1029/JA089iA01p00195.
Pfaff, R., C. Liebrecht, J.-J. Berthelier, M. Malingre, M. Parrot, and J.-P. Lebreton (2008), DEMETER satellite observations of plasma irregularities in the topside ionosphere at low, middle, and sub-auroral latitudes and their dependence on magnetic storms, in *Midlatitude Ionospheric Dynamics and Disturbances*, vol. 181, edited by P. M. Kintner et al., pp. 297–310, AGU, Washington, D. C.
Pickett, J. S., et al. (2010), Cluster observations of EMIC triggered emissions in association with Pc1 waves near Earth's plasmapause, *Geophys. Res. Lett.*, *37*, L09104, doi:10.1029/2010GL042648.
Rauch, J. L., and A. Roux (1982), Ray tracing of ULF waves in a multicomponent magnetospheric plasma—Consequences for the generation mechanism of ion cyclotron waves, *J. Geophys. Res.*, *87*, 8191–8198, doi:10.1029/JA087iA10p08191.
Russell, C., R. Holzer, and E. Smith (1970), OGO3 observations of ELF noise, *J. Geophys. Res.*, *75*, 755–768.
Sakaguchi, K., Y. Kasahara, M. Shoji, Y. Omura, Y. Miyoshi, T. Nagatsuma, A. Kumamoto, and A. Matsuoka (2013), Akebono observations of EMIC waves in the slot region of the radiation belts, *Geophys. Res. Lett.*, *40*, 5587–5591, doi:10.1002/2013GL058258.
Santolík, O., J. S. Pickett, D. A. Gurnett, M. Maksimovic, and N. Cornilleau-Wehrlin (2002a), Spatiotemporal variability and propagation of equatorial noise observed by Cluster, *J. Geophys. Res.*, *107*(A12), 1495, doi:10.1029/2001JA009159.
Santolík, O., J. S. Pickett, D. A. Gurnett, and L. R. O. Storey (2002b), Magnetic component of narrow-band ion cyclotron waves in the auroral zone, *J. Geophys. Res.*, *107*(A12), 1444, doi:10.1029/2001JA000146.

Santolík, O., M. Parrot, and F. Lefeuvre (2003), Singular value decomposition methods for wave propagation analysis, *Radio Sci.*, *38*(1), 1010, doi:10.1029/2000RS002523.

Sawada, A., Y. Kasahara, M. Yamamoto, I. Kimura, S. Kokubun, and K. Hayashi (1991), ELF emissions observed by the EXOS-D satellite around the geomagnetic equatorial region, *Geophys. Res. Lett.*, *18*(2), 317–320, doi:10.1029/91GL00040.

Summers, D., and R. Thorne (2003), Relativistic electron pitch-angle scattering by electromagnetic ion cyclotron waves during geomagnetic storms, *J. Geophys. Res.*, *108*(A4), 1143, doi:10.1029/2002JA009489.

Temerin, M., and R. Lysak (1984), Electromagnetic ion cyclotron mode (ELF) waves generated by auroral electron precipitation, *J. Geophys. Res.*, *89*(A5), 2849–2859.

Thorne, R. M., and R. B. Horne (1997), Modulation of electromagnetic ion cyclotron instability due to interaction with ring current O^+ during magnetic storms, *J. Geophys. Res.*, *102*, 14,155–14,164, doi:10.1029/96JA04019.

Usanova, M. E., I. R. Mann, I. J. Rae, Z. C. Kale, V. Angelopoulos, J. W. Bonnell, K.-H. Glassmeier, H. U. Auster, and H. J. Singer (2008), Multipoint observations of magnetospheric compression-related EMIC Pc1 waves by THEMIS and CARISMA, *Geophys. Res. Lett.*, *35*, L17S25, doi:10.1029/2008GL034458.

Usanova, M. E., I. R. Mann, J. Bortnik, L. Shao, and V. Angelopoulos (2012), THEMIS observations of electromagnetic ion cyclotron wave occurrence: Dependence on AE, SYMH, and solar wind dynamic pressure, *J. Geophys. Res.*, *117*, A10218, doi:10.1029/2012JA018049.

Yizengaw, E., H. Wei, M. Moldwin, D. Galvan, L. Mandrake, A. Mannucci, and X. Pi (2005), The correlation between mid-latitude trough and the plasmapause, *Geophys. Res. Lett.*, *32*, L10102, doi:10.1029/2005GL022954.

Young, D., S. Perraut, A. Roux, C. de Villedary, R. Gendrin, G. K. A. Korth, and D. Jones (1981), Wave particle interactions near Ω_{He+} observed on GEOS 1 and 2, 1, propagation of ion cyclotron waves in He^+-rich plasma, *J. Geophys. Res.*, *86*, 6755–6772.